International Journal of Engineering & Technology, 7 (4) (2018) 4922-4929

International Journal of Engineering & Technology

Website: www.sciencepubco.com/index.php/IJET
doi: 10.14419/ijet.v7i4.15768
Research paper

Convex optimization and greedy iterative algorithms for dictionary learning in the presence of Rician noise

M. V. R. Manimala [1] *, C. Dhanunjaya Naidu [2], M. N. Giri Prasad [1]

[1] JNTUA, Ananthapuramu, India
[2] VNRVJIET, Hyderabad, India
**Corresponding author E-mail: svrmanimala_ece@mvsrec.edu.in*

Abstract

Compressive Sensing (CS) is the emerging trend of recovering signal/image accurately from samples acquired at a rate far below the Nyquist rate. MR imaging provides a natural fit for applying CS as they can be sparsely represented in the transform domain. Magnitude MR images are corrupted by noise which follows Rician distribution and is difficult to remove as it is image dependent. Sparse coding is an important stage in dictionary learning. In this paper an attempt is being made to bring out a sparse coding technique which can provide better reconstruction in the presence of Rician noise. Greedy iterative algorithms and l_1 convex solutions are widely used for sparse coding. In the present work, performance of greedy algorithms, namely, Orthogonal Matching Pursuit (OMP) and Compressive Sampling Matching Pursuit (CoSaMP) have been evaluated and compared with convex techniques viz. Basis Pursuit (BP) and Least Absolute Shrinkage and Selection Operator (LASSO) in the sparse coding stage of an adaptive patch-based dictionary learning. Experiments have been carried out by varying Rician noise level from 0 to 30 and sparsity threshold per patch on MR images, acquired by employing various sampling schemes. Results show that greedy algorithms achieve higher PSNR and have very high computational speed compared to convex techniques when the MR images are corrupted with Rician noise.

Keywords: *Compressive Sensing; Convex Techniques; Greedy Iterative Algorithms; Magnetic Resonance Imaging.*

1. Introduction

Compressive Sensing (CS) is the current signal acquisition technique that is rapidly replacing the conventional sampling done at Nyquist rate. CS can recover signals accurately from samples that are lesser than the Nyquist rate by exploiting the sparsity of the signal in some transform domain or dictionary [1,2]. Other conditions for CS recovery include incoherence of the measurements with respect to the transform and a non-linear reconstruction procedure which is computationally expensive. CS offers applications in various domains, such as medical imaging, where the scan time can be reduced, communication and networks for sparse channel estimation and to acquire data for large wireless sensor networks [3].

In MR Imaging, signal is acquired in 2D frequency space known as k-space and MR image is reconstructed from the k-space data by using Fourier transform. CS is useful in MR imaging as it reduces the scan time and MR images satisfy the sparsity criteria necessary for CS. In this article CS paradigm has been employed for MR imaging and an investigation of the performance of sparse codes has been performed for an adaptive patch based dictionary learning developed by Saiprasad Ravishankar et al in [1].

Although various sparse recovery strategies exist for the present work, two classes of sparse recovery techniques have been analyzed which include greedy iterative algorithms and convex optimization techniques. Algorithms analyzed under greedy techniques are (i) Orthogonal Matching Pursuit (OMP) [4], (ii) Compressive Sampling Matching Pursuit (CoSaMP) [5]. Under convex solutions following techniques are analyzed: (i) Basis Pursuit (BP) [6], [7], (ii) Least Absolute Shrinkage and Selection Operator (LASSO) [8], [9]. Sparse recovery is an important stage in dictionary learning (DL). An efficient DL algorithm based on K-SVD was proposed by Aharon et al in [10]. Recently an analysis of these sparse recovery techniques for dictionary learning MRI (DLMRI) has been carried out in [11]. An adaptive patch based dictionary [1] is employed to enhance the sparsity, as it captures the local features of the images better than a global sparsifying transform [10]. In [1] performance of DLMRI has been analyzed in the presence of Gaussian noise.

Noise in MR images arises due to thermal variations in the patient and to certain extent from the acquiring system. The presence of noise degrades the resolution and contrast of the image and it becomes difficult to interpret the data and analyse the results. Computation of MRI is done by considering both real and imaginary images. Magnitude MR images are corrupted by noise which follows Rician distribution and leads to Rayleigh distribution in the absence of MR signal, whereas, in the high intensity regions, it follows Gaussian distribution [12]. As Rician noise is image dependent, it becomes difficult to remove it. In [13] jittered undersampling was used to denoise seismic data, which employs the benefits of random sampling and controls maximum gap size. Pre-smoothing non local means filter combined with image transformation was used to denoise MR images corrupted with Rician noise in [14]. Javier et al proposed multiple dictionaries as a prior in [15] for relaxed analysis based sparsity to restore images corrupted with Additive White Gaussian Noise. In [16] MR images were denoised by estimating the prior and considering the Rician noise model. In their work, Empirical Bayes estimation was used to model a prior in a non-parametric Markov Random Field, but the sparsity inherent in the MR images was not exploited. In [17] a Bayesian nonparametric model was used to reconstruct MR images from highly undersampled k-space data. Here nonparametric dictionary learning was

employed to reconstruct the images and the results were analyzed by varying patch sizes and sparsity for Gaussian noise. Although comparison of greedy and convex solutions exists, performance analysis with the Rician noise in an adaptive patch based dictionary learning framework is less studied.

In the present work, performance of DLMRI with sparse recovery algorithms OMP, CoSaMP, BP and LASSO, has been examined under the influence of Rician noise. An attempt has been made to present a comprehensive evaluation of greedy and convex solutions. Experimentation has been carried out on various MR images by varying Rician noise level for various undersampling schemes and sparsity levels. The rest of the paper is organized as follows. Concept of CS and its recovery schemes has been described in section 2. Under CS recovery, greedy iterative algorithms (OMP, CoSaMP) and convex techniques (BP, LASSO) have been discussed. Noise reduces the intelligible information of the images and is a major problem in the medical images. Section 3 describes the types of noises that affect the MR images. Section 4 presents dictionary learning and illustrates the present work. Experimentation and results are mentioned in Section 5. Section 6 concludes this paper with future scope.

2. Compressive sensing

Compressive Sensing is the problem of finding unknown x from the set of measurements y by solving the following

$$\min_{x} \quad \| \Psi x \|_0 \quad \text{s.t.} \quad \Phi x = y \tag{1}$$

Where $x \in C^n$ is a vector representing image, $y \in C^m$ represents the measurements, $\Phi \in C^{m \times n}$ is the sensing or measurement matrix with $m << n$. $\psi \in C^{n \times n}$ is the domain in which the signal/image is sparse and is termed as sparsity domain. Typically ψ is orthonormal and $\Psi x = z$, hence the above eq. becomes

$$\min_{z} \|z\|_0 \quad \text{s.t} \quad \Phi \psi^{H} z = y \tag{2}$$

Here $(\cdot)^H$ denotes Hermitian operation. Finding l_0 norm is NP hard hence the above equation can be solved by replacing l_0 norm with its convex relaxation, the l_1 norm [1,6]. Alternatively, greedy algorithms such as OMP, CoSaMP can be employed to solve this problem. A brief review of the greedy algorithms and convex techniques is presented next.

2.1. Orthogonal matching pursuit

Tropp et al in [4] proposed OMP, which solves the CS reconstruction problem iteratively. A k-sparse signal $x \in \mathrm{R}^n$ can be represented by an m-dimensional measurement vector y using a measuring matrix $\Phi \in \mathrm{R}^{m \times n}$ with columns $\phi_1, \phi_2, \phi_3, \ldots \phi_n$. In each iteration OMP picks a column of Φ that maximizes the correlation with the measurements y i.e. least mean square error is minimized at each step. The selected row is then subtracted from the measurements y to form the residual signal. Iterations are carried out on the residual signal until the entire support for the signal is identified. k-iterations are required to identify the entire support. In OMP same atom can never be selected twice as residual is always orthogonal to the atoms already selected [4].

2.2. Compressive sampling matching pursuit

Needell et al proposed CoSaMP in [5], a variant of OMP which proves to be useful when the signal is not much sparse and recovery is computationally expensive. Every iteration consists of identifying largest 2k components of the signal proxy along with the index, which is then added to the support set. Least squares problem is solved on the merged set of components to estimate the target signal. Pruning stage consists of retaining the largest k entries. Lastly, samples are restored to reflect the residual. These steps are repeated till the halting criterion is reached [5].

2.3. Basis pursuit

Donoho et al have solved sparse problem in [6] by using BP which is done by replacing l_0 norm with its convex relaxation l_1 norm. When it is carried under noiseless conditions, it is represented by

$$\min_{z} \|z\|_1 \quad \text{s.t} \quad \Phi \psi^{H} = y \tag{3}$$

BP may not lead to sparse solution every time, but under right conditions it can provide a sparse solution or even sparsest solution [6]. Major disadvantage with BP is that, it leads to non zero entries at every position even though the values may be very small. LASSO overcomes this disadvantage and is described next.

2.4. Least absolute shrinkage and selection operator

Tibshirani proposed Least Absolute Shrinkage and Selection Operator (LASSO) [8] which performs variable selection and shrinkage. The 'lasso' minimizes the residual sum of squares subject to the sum of the absolute value of the coefficients being less than a constant. BP minimizes the l_1 norm, whereas LASSO places restriction to its value. LASSO can be employed when CS measurements are noisy which is represented by

$$\min \quad \| \Phi x - y \|_2 \ \text{s.t} \ \| x \|_1 < \lambda \tag{4}$$

Ordinary least squares (OLS) has drawbacks of prediction accuracy and representation. Shrinking or setting some coefficients to zero improves prediction accuracy and interpretation. Two techniques for improving the OLS estimates are subset selection and ridge regression but both have drawbacks. Subset selection results in interpretable model but has poor prediction accuracy, as regressors are either retained or dropped from the model. Hence minor changes in data lead to different models being selected which affects the prediction accuracy. Ridge regression shrinks coefficients but does not set any coefficients to zero, hence it is stable but cannot provide an accountable model [8]. These drawbacks are overcome in LASSO as it adapts good features of both subset selection and ridge regression. LASSO shrinks some coefficients while others are set to zero.

3. Noise models

Reconstruction of MR images is done by acquiring k-space data from real and imaginary channel, which may be corrupted by additive Gaussian noise. The prime source of Gaussian noise is the thermal noise from the patient and to certain extent from the acquisition hardware.

3.1. Gaussian noise

For a random variable x , with mean μ and variance σ^2, the Gaussian distribution is given by the following equation

$$P(x) = \frac{1}{\sigma\sqrt{2\pi}} \; e^{-(x-\mu)^2/(2\sigma^2)} \tag{5}$$

MR image is reconstructed from the k-space data by applying inverse Fourier Transform. The shape of the noise distribution is preserved by transformation and hence it remains Gaussian [12]. Magnitude images are obtained from MR images by calculating absolute value pixel by pixel, (m [i, j]) from the real and imaginary images which is given by

$$|m[i,j]| = \sqrt{m[i,j]_{re}^{\,2} + m[i,j]_{im}^{\,2}}$$

Where

$$m[i,j]_{re} = s[i,j]\cos(\phi) + n_{re}[i,j]$$

And

$$m[i,j]_{im} = s[i,j]\sin(\phi) + n_{im}[i,j] \tag{6}$$

Here m[i,j] represents the magnitude signal in the pixel [i,j], s[i,j] is the signal component, ϕ is the phase angle and n represents the noise contribution to the real and imaginary part in the given pixel [i,j]. Hence magnitude image has a modified noise distribution and does not contain any information about the phase angle ϕ. The noise in magnitude image depends on signal and follows Rician distribution.

3.2. Rician noise

Rician probability function for the noise in the magnitude images is given by

$$P(m) = \frac{m}{\sigma^2} \; e^{-(m^2+s^2)/2\sigma^2} \; \hat{I}_0\left[\frac{s.m}{\sigma^2}\right] \tag{7}$$

Where $\hat{I}_0$ represents the modified zeroth order Bessel function of the first kind, m represents the measured pixel intensity and s is the pixel intensity in the noiseless image [12]. Rician noise reduces the image contrast as it introduces signal dependent bias to the data. When $|s| = 0$, the above equation reduces to Rayleigh distribution.

$$P(m) = \frac{m}{\sigma^2} \; e^{-m^2/2\sigma^2} \tag{8}$$

Regions in the image that has no MR signal have Rayleigh distribution. Hence noise in the low intensity regions of magnitude image tends to Rayleigh distribution and in high intensity regions tends to Gaussian distribution.

4. Dictionary learning

Global image sparsity can be exploited for CS reconstruction, but is limited by the degree of undersampling it can achieve. In the recent past adaptive patch based dictionaries were developed, that adapted to the data to give higher sparsities and hence provided higher undersampling rates with good quality of reconstruction. Adapting the dictionary to the data is termed as dictionary learning. Each column vector in the dictionary is known as atom. A dictionary is termed as overcomplete if the number of patches (atom) is greater than the patch size. When the patch size is equal to the number of atoms, such a dictionary is termed as complete. Dictionary learning MRI (DLMRI) was developed in [1] which employs an adaptive patch based dictionary to reconstruct MR images. DLMRI reconstructs MR images iteratively, by first training the dictionary using K-SVD [10] and next, it employs the trained dictionary to sparse code all the patches of the image using OMP. Sparse coding is a crucial stage in K-SVD. In [11], sparse coding stage for DLMRI was analyzed by employing OMP, CoSaMP and BP with respect to the undersampling limit, number of iterations, operational complexity and various sampling schemes.

The present work builds on the work of Ravishankar et al in [1]. In this article, OMP, CoSaMP, LASSO and BP are considered for sparse coding of patches in DLMRI. Performance of these algorithms is evaluated with respect to Rician noise for brain and knee image by varying sampling schemes and sparsity threshold per patch (m/k).

5. Results

Experimentation has been done on sparse coding stage of DLMRI algorithm with four sparse coding techniques namely OMP, CoSaMP (greedy iterative algorithms), BP and LASSO (convex optimization technique) for brain, C-spine, L-spine and knee image corrupted with Rician noise. Parameter setting for the algorithm and metrics employed are given in the next part.

5.1. Parameters

Reconstruction is quantified by Peak Signal to Noise Ratio (PSNR) in decibels (dB) and High Frequency Error Norm (HFEN). PSNR is computed as the ratio of peak intensity value of reference image to the reference image. HFEN signifies the quality of reconstruction of edges and fine edges. PSNR0 represents zero filled reconstruction. To analyze the effect of sparsity on PSNR and runtime, experiments were performed by varying the ratio m/k, where 'm' represents the number of measurements per patch and 'k' is the sparsity threshold per patch.

All the computations were done on an Intel Core i5 CPU at 2.3 GHz and 12 GB memory, with 64-bit Windows 8 operating system. All implementations have been coded in Matlab R2016b.

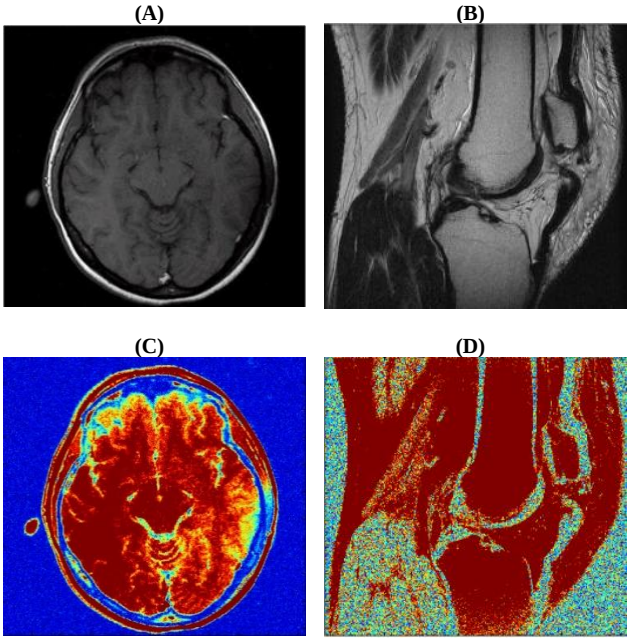

Fig. 1: Reference Images (A) Brain [1], (B) Knee (C) Brain Image Corrupted with Rician Noise (Noise Level 5.2) (D) Knee Image Corrupted with Rician Noise (Noise Level 20.2).

Design parameters for the algorithm are the patch size $\sqrt{m}$ x$\sqrt{m}$ (number of measurements), sparsity threshold per patch k, λ is a factor that signifies data consistency in the presence of noise. N is the total number of overlapping patches in the image, δ represents fraction of patches used to train the dictionary and J is the number of iterations in learning. Algorithm has been tested with three sampling schemes namely 7.11 fold Pseudoradial sampling, 4-fold random sampling and 4-fold Cartesian sampling for brain and knee image. Fig.1 shows the reference images of brain and knee.
DLMRI is an iterative algorithm. In the present work, DLMRI iterations has been fixed to one and DL stage of DLMRI employs 5 iterations of K-SVD for all the results. l_1 magic toolbox [7] and SparseLab [9] has been employed for implementing BP and LASSO respectively.

5.2. Effect of sampling scheme on brain image

Experiments have been carried out by varying noise level from 5.2 to 30.2 on brain [1] to study the effect of sampling scheme on the performance of the four sparse coding techniques in the DL framework. Fig. 2 Illustrates the PSNR plots for the brain image with various sampling schemes and a fixed m/k value of 5. Fig. 2a shows 7-fold pseudoradial undersampling of the k-space and Fig. 2b depicts the corresponding PSNR obtained by varying noise level from 5.2 to 30.2 for four sparse coding techniques. It has been observed that for pseudoradial sampling, CoSaMP and LASSO achieves better reconstruction at low noise levels, whereas for Cartesian (Fig. 2d) and random (Fig. 2f) sampling, OMP and CoSaMP achieves higher PSNR. For high noise levels all the algorithms achieve similar PSNR.
The artifacts mentioned above have been observed for all the sparse coding techniques considered in this work. Due to space limitation, reconstructed images for CoSaMP, BP and LASSO have not been shown. Experimentation shows that, for pseudoradial sampling, CoSaMP and LASSO achieves better reconstruction at low noise levels, whereas for Cartesian and random sampling, OMP and CoSaMP achieves higher PSNR. For high noise levels all the algorithms achieve similar PSNR.

5.3. Effect of sampling scheme on knee image

Fig. 3 depicts the effect of Rician noise on the knee image. Experiments were done on knee image by varying the noise level and sampling scheme. As in Fig. 2, m/k value has been fixed to 5 for all the simulations in Fig. 3.

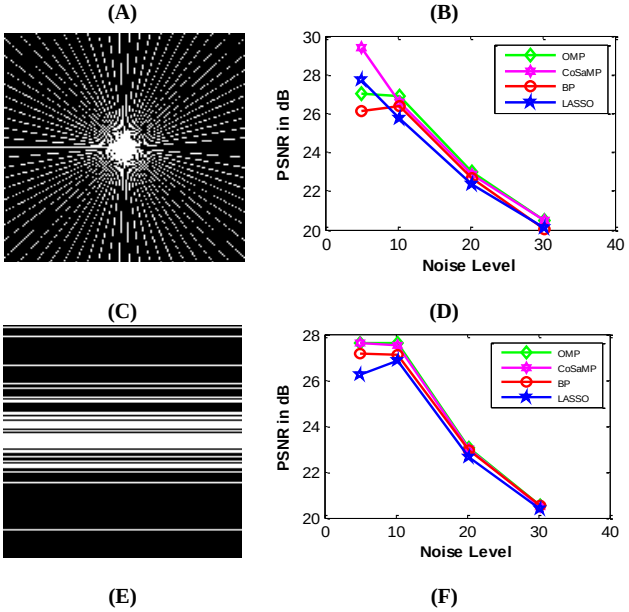

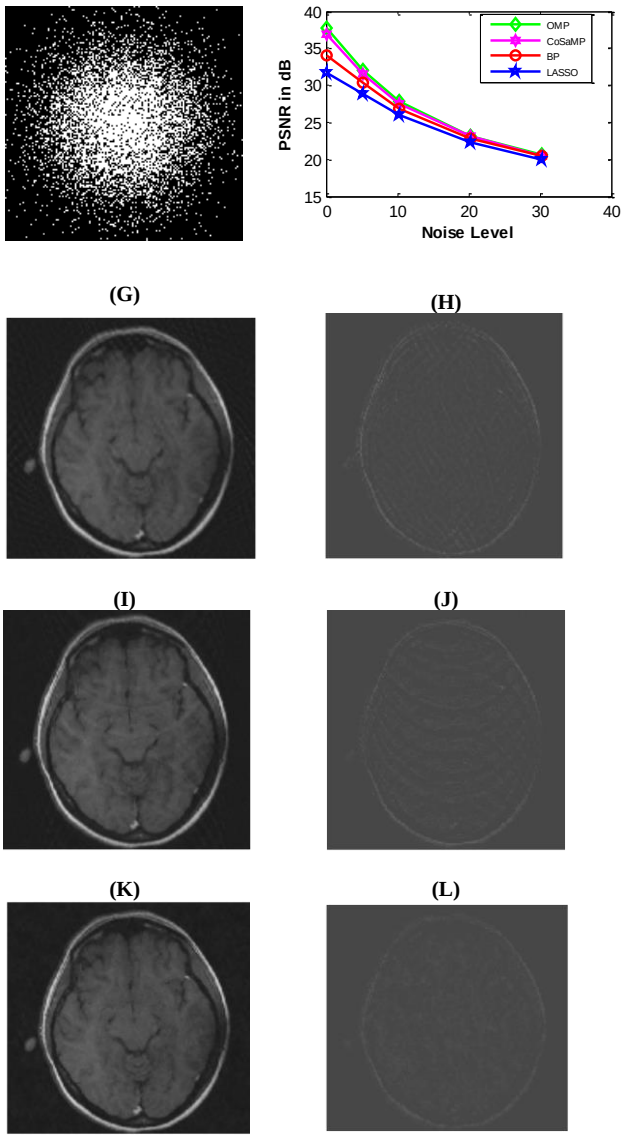

Fig. 2: PSNR Versus Noise Level for OMP, Cosamp, BP and LASSO (A) 7.11-Fold Pseudoradial Sampling Mask in K-Space [1] (B) PSNR vs. Noise with Pseudoradial Sampling (C) 4-Fold Variable Density Cartesian Sampling [1]. (D) PSNR Plot for Cartesian Sampling (E) 4-Fold Random Undersampling [1]. (F) PSNR Plot with 4-Fold Random Undersampling (G) OMP: Reconstruction with Pseudoradial Sampling and Noise 5.2 (H) OMP: Reconstruction Error with Pseudoradial Sampling (I) OMP: Reconstruction With Cartesian Sampling And Noise 5.2 (J) OMP: Reconstruction Error with Cartesian Sampling (K) OMP: Reconstruction with 4 Fold Random Sampling and Noise 5.2 (L) OMP: Reconstruction Error with Random Sampling.

In Fig. 3a and 3b pseudoradial at 7.11 undersampling, has been used. When the Rician noise level is increased from 5.2 to 10.2, PSNR increases by about 1dB for all the sparse recovery techniques as shown in Fig. 3a. Further increase in the noise level causes the PSNR to decrease and is similar for all the sparse recovery techniques. Fig. 3b depicts the corresponding HFEN variation. Contrary to the PSNR, HFEN increases with the increase in noise. Hence, it can be inferred that as noise increases, accuracy in the reconstruction of edges, reduces.
PSNR plots in Fig. 3c are obtained by randomly sampling the k-space at 4 fold undersampling. For low noise condition i.e. below 5, PSNR for CoSaMP is observed to be higher than the corresponding values of OMP, LASSO and BP. As the noise increases, OMP obtains marginally higher PSNR compared to other, however it deteriorates as the noise level increases beyond 20.

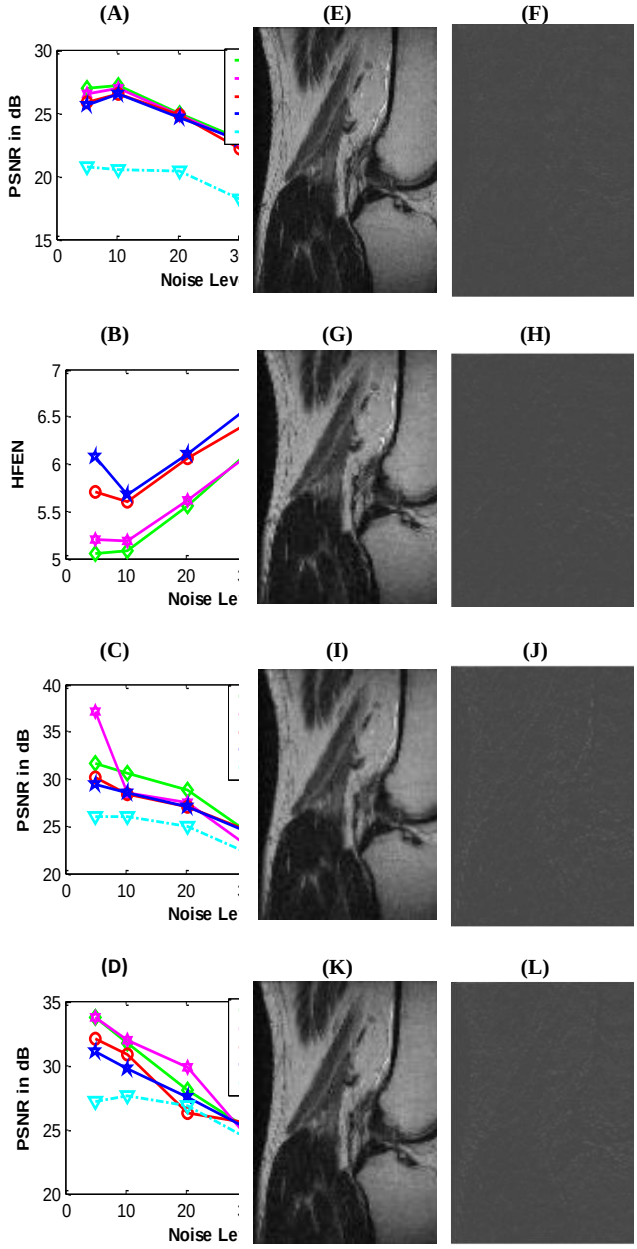

Fig. 3: Knee Image:Rician Noise Analysis with Various Sampling Schemes and M/K=5 (A) 7.11 Fold Pseudoradial Sampling: PSNR Vs. Noise Level (B) 7.11 Fold Pseudoradial Sampling: HFEN vs Noise (C) 4 Fold Random Sampling: PSNR vs. Noise Level (D) 4 Fold Cartesian Sampling: PSNR vs. Noise Level (E) Cartesian Sampling, OMP: Reconstructed Image (Noise Level=5.2) (F) OMP: Reconstruction Error (G) Cartesian Sampling, Cosamp: Reconstructed Image (Noise Level=5.2) (H) Cosamp: Reconstruction Error (I) Cartesian Sampling, LASSO: Reconstructed Image (Noise Level=5.2) (J) LASSO: Reconstruction Error (K) Cartesian Sampling, BP: Reconstructed Image (Noise Level=5.2) (L) BP: Reconstruction Error.

PSNR plot for knee image reconstructed from Cartesian sampling at 4 fold undersampling is shown in Fig. 3d. PSNR for OMP and CoSaMP is observed to be similar for lower levels of noise (0-5.2), but as the noise level is increased to 10, performance of OMP drops sharply compared to CoSaMP. At noise level of 20, PSNR for CoSaMP (29.84 dB) is about 2dB higher than that of OMP (28 dB). Under noiseless condition OMP and CoSaMP obtains a PSNR of 33.7 dB, corresponding values of PSNR for BP and LASSO are 32 dB and 31dB respectively. At the noise level of 30.2, all the algorithms attain similar PSNR of about 23 dB. Reconstruction for noise level 5.2 with OMP and CoSaMP is shown in Fig. 3e and 3g respectively. Corresponding reconstruction error is given in 3f and 3h. Reconstruction error with OMP and CoSaMP is seen to be very low. Fig. 3i and 3k are the reconstruction from LASSO and BP respectively. Fig. 3j and 3l represent the corresponding reconstruction error.

Experimental results demonstrate that, for pseudoradial sampling there is not much difference in the PSNR obtained by the four algorithms. For random sampling, CoSaMP achieves better PSNR than OMP for low noise. However at high noise, OMP provides better PSNR compared to other algorithms. For Cartesian sampling CoSaMP achieves comparatively higher PSNR. Although there is not much difference in the visual quality, HFEN values and the reconstruction error indicate that the error in the reconstruction of edges is more in the case of LASSO and BP. Reconstruction shows that, brighter regions are more affected by the Rician noise than the darker region.

5.4. Analysis with m/k

Fig. 4 depicts the variations in PSNR, HFEN and runtime with m/k for brain image acquired with 4-fold random sampling of k-space. Noise has been varied from 0 to 30.2 and is represented by N in the plots. m/k has been varied from 2 to 7 in steps of 1 for all the simulations in this section.

In Fig. 4a and 4b, OMP and CoSaMP has been employed respectively, for sparse coding. As m/k increases there is a slight increase in the PSNR value. For OMP under noiseless conditions PSNR increases by 0.6 dB (37.22 dB to 37.82 dB) with m/k, whereas for CoSaMP it decreases by 0.13 dB (37.03 to 36.9 dB). Variation in the PSNR with m/k is greater for convex optimization techniques. PSNR falls by about 3.86 dB (35.56 dB to 31.7 dB) for LASSO, as m/k value is raised. Corresponding value for BP is 2.5 dB (35.71 dB to 33.21 dB).

Runtime for CoSaMP is observed to be 46.18 sec for m/k=2 and 210 sec for m/k=7. Corresponding values for LASSO is 19.14 sec and 168.49 sec. In the case of BP runtime is around 90 sec for m/k=2 and it increases to 2227 sec for m/k=7. As the noise level is reduced, the runtime decreases marginally, not shown here.

For noisy measurements, it has been observed that the variations in PSNR with respect to m/k decreases. For noise level of 10.2, PSNR increases for OMP and CoSaMP by 0.26 dB and 0.22 dB respectively, whereas for LASSO (Fig. 4c) and BP (Fig. 4d) it decreases by 1.51 dB and 0.57 dB respectively. As the noise level increases, the variation in the PSNR reduces for all the algorithms. As Rician noise is signal dependent, it is difficult to remove this from the image.

Fig. 4e presents the runtime variation for four algorithms with m/k at a fixed noise level of 30.2. As m/k increases, computations also increase thereby increasing the runtime of the algorithm. The plot indicates that, the runtime is very low for m/k=2 and 3, for higher values of m/k runtime increases for all the algorithms. The runtime for BP in particular, is very high when compared with other techniques. Runtime for OMP has been noted to be 16.21 sec for m/k=2 and it increases to 162.35 sec for m/k=7. Similar trends follow for CoSaMP and LASSO.

The relation between PSNR and HFEN with m/k variation is illustrated in Fig. 4f. OMP with noiseless measurements has been employed for this plot. It is seen that PSNR increases from 37.2 dB to 37.8 dB with m/k, whereas HFEN decreases from 1.09 to 0.952.

Experimental results demonstrate that runtime and computational complexity increases with m/k. BP has a disadvantage of high runtime. PSNR varies marginally with m/k for all the algorithms. High value of PSNR and low value of HFEN is desirable for good reconstruction. Other results for HFEN are not shown here. High PSNR indicates a low HFEN.

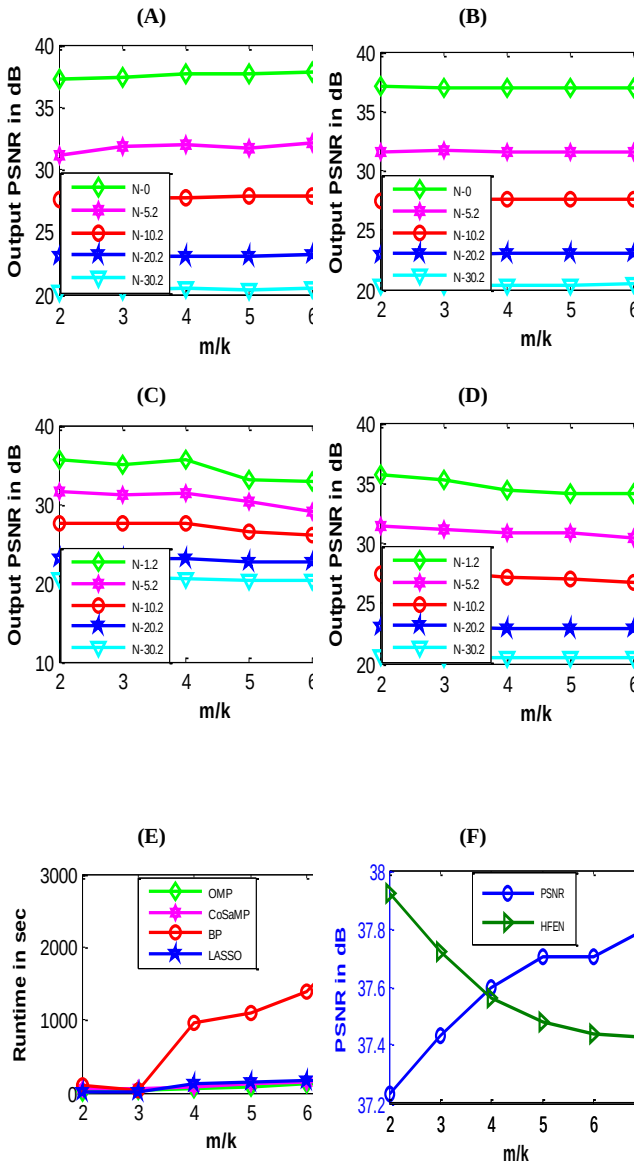

Fig. 4: Brain: PSNR Versus M/K for Rician Noise (A) OMP (B) Cosamp (C) LASSO (D) BP (E) Runtime Versus M/K (F) PSNR and HFEN Versus M/K.

5.5. Experimentation with in vivo k-space data

Fig. 5. (a) and 5(c) Presents in vivo k-space data of sagittal T2 weighted C-spine and L-spine respectively. Fig.5 (e) shows the sagittal T1 weighted knee image (from mridata.org) and Fig. 5. (g) shows the axial MR image of brain. Experimentation has been performed on these images by corrupting it with a Rician noise level of 11.09 and subsequently sampling it in k-space with 4-fold random undersampling (Fig.2 (e)). OMP and CoSaMP have been evaluated with 5 iterations of DLMRI as they are greedy iterative algorithms, where as BP and LASSO were implemented with single iteration of DLMRI as the performance of the convex optimization does not improve with iterations. K-SVD iterations have been fixed to 5 for all the simulations. Reconstructed images with OMP are shown in Fig. 5.(b), 5.(d), 5.(f) and 5.(h). The numerical results are presented in Table 1. Results show that OMP and CoSaMP obtain marginally higher PSNR compared to BP and LASSO. Computation time is least for OMP. Lowest HFEN is also observed with OMP which confirms the better reconstruction quality with OMP compared to other sparse coding techniques under consideration.
Table 2 Illustrates the results obtained for the brain image (Fig. 1 a). Experimentation has been performed on the brain image by varying the noise level from 5.2 to 30.2 for three sampling schemes namely 7-fold pseudoradial, 4-fold Cartesian and 4-fold random undersampling. Sparse coding stage in the DLMRI algorithm has been evaluated by considering OMP, CoSaMP, BP and LASSO. m/k ratio has been fixed to 5 for the results in Table 2 and metrics evaluated are PSNR (Peak Signal to Noise Ratio), HFEN (High Frequency Error Norm) and Runtime. PSNR0 indicates the zero filled PSNR.

Table 1: PSNR0 (Zero Filled PSNR), PSNR, HFEN and Runtime with OMP, Cosamp, BP and LASSO for in-Vivo Data of C-Spine, L-Spine, Brain and Knee

	OMP	CoSaMP	BP	LASSO
C-Spine Image (Fig. 5(a))				
PSNR0 in dB	24.1	24.1	24.13	24
PSNR in dB	30.57	30	28.13	28.24
HFEN	2.23	2.62	3.18	3.09
Runtime in seconds	79	126	908	107
L-Spine Image (Fig. 5(b))				
PSNR0 in dB	24.67	24.65	24.58	24.54
PSNR in dB	29.53	29.17	27.71	27.22
HFEN	2.25	2.66	3.05	3.11
Runtime in seconds	79.7	125	892	112
Knee Image (Fig. 5(c))				
PSNR0 in dB	25.32	25.65	25.31	25.67
PSNR in dB	31.53	30.98	30.38	30.22
HFEN	2.02	2.37	2.38	2.49
Runtime in seconds	49	132	925	91
Brain Image (Fig. 5 (d))				
PSNR0 in dB	23.49	23.81	24.55	24.85
PSNR in dB	28.79	28.51	28.26	28.18
HFEN	2.25	2.52	2.67	2.55
Runtime in seconds	57	140	864	97

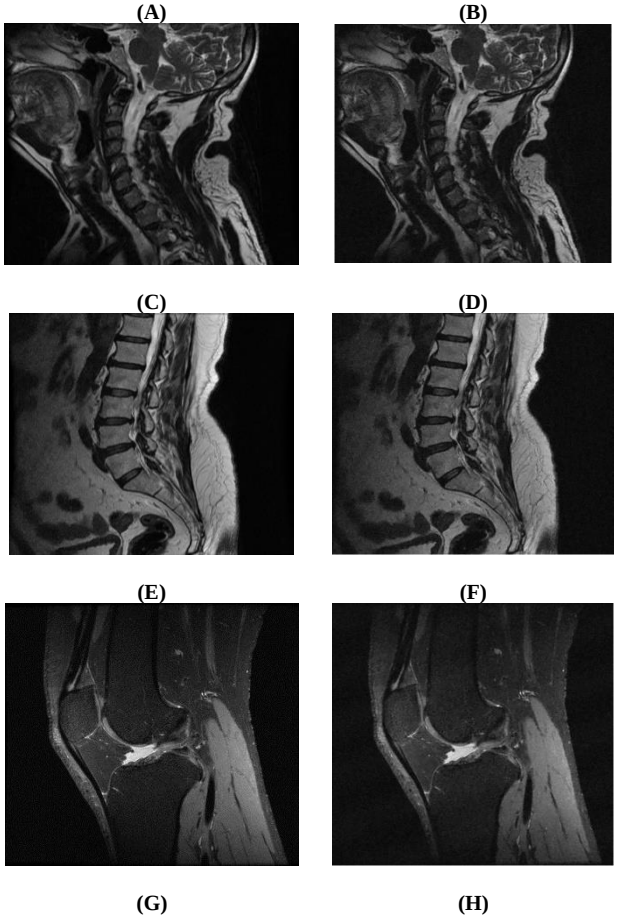

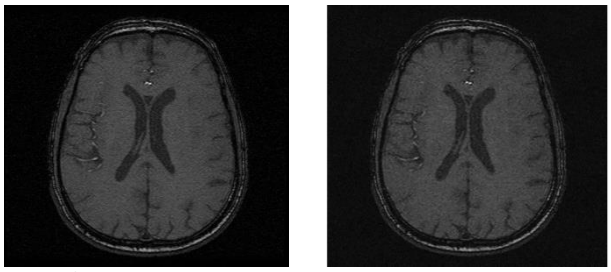

Fig. 5: Reference Images (A) C-Spine (C) L-Spine (E) Knee (G) Brain (B) Reconstructed C-Spine (D) L-Spine (F) Knee (H) Brain.

Low runtime indicates fast convergence of the algorithm. From the results in Table 2, it can be seen that, CoSaMP obtains higher PSNR at low noise levels (5.2). For higher noise, OMP achieves highest PSNR and lowest HFEN. Lowest runtime has been observed with OMP. A runtime of about 80 sec has been noted for CoSaMP with psuedoradial and Cartesian sampling whereas for random sampling a runtime of about 120 sec has been noted. LASSO has runtime of around 120 sec. Highest runtime of about 1050 sec has been observed with BP.

6. Conclusion and future scope

This article presents the comparison of greedy algorithms (OMP, CoSaMP) and convex techniques (BP, LASSO) in DLMRI for various aspects that include sampling scheme, m/k variation and varied noise levels. In the presence of Rician noise, pseudoradial sampling displays streaks, Cartesian sampling exhibits aliasing artifacts whereas random sampling overcomes these artifacts however, displays some blurring and this was observed with all the.

Table 2: PSNR, HFEN and Runtime with Three Different Sampling Schemes for Brain Image

Parameter	Algorithm	Noise Level :5.2	Noise Level :10.2	Noise Level :20.2	Noise Level :30.2
7_Fold Pseudoradial Sampling, m/k=5					
PSNR0 (dB)	Zero filled	24.35	23.71	20.58	18.13
Output PSNR (dB)	OMP	26.99	26.89	22.96	20.46
	CoSaMP	29.39	26.6	22.86	20.46
	BP	26.11	26.36	22.67	20.06
	LASSO	27.72	25.72	22.35	20.1
HFEN	OMP	3.6	3.63	4.24	4.84
	CoSaMP	3.49	3.86	4.38	4.9
	BP	4.27	4.08	4.65	5.05
	LASSO	4.25	4.53	5.1	5.44
Runtime in Seconds	OMP	16.84	16.32	27.57	60.05
	CoSaMP	81.97	82.86	86.74	79
	BP	1025.53	1019	1025	1100
	LASSO	116.74	111.74	121.12	119.22
4_Fold Cartesian Sampling					
PSNR0 (dB)	Zero filled	26.13	25.97	22.11	19
Output PSNR (dB)	OMP	27.61	27.6	23.07	20.54
	CoSaMP	27.63	27.51	23.02	20.48
	BP	27.14	27.11	22.93	20.55
	LASSO	26.24	26.84	22.66	20.37
HFEN	OMP	2.27	2.27	3.34	4.27
	CoSaMP	2.39	2.43	3.47	4.32
	BP	2.86	2.78	3.7	4.46
	LASSO	3.61	3.09	4.21	4.81
Runtime in Seconds	OMP	19.80	20.11	36.35	64.3
	CoSaMP	79.81	84.22	82.37	85.37
	BP	1063.76	1054	1080	1050
	LASSO	121.12	114.95	127.6	127.17
4-Fold Random Sampling					
PSNR0 in dB	Zero filled	28.5	25.92	21.88	19.21
Output PSNR In dB	OMP	31.75	27.89	23.12	20.42
	CoSaMP	31.51	27.56	23.05	20.4
	BP	30.88	27.09	22.89	20.47
	LASSO	30.35	26.49	22.65	20.33
HFEN	OMP	1.49	2.12	3.48	4.64
	CoSaMP	1.76	2.42	3.66	4.69
	BP	2.16	2.8	3.8	4.46
	LASSO	2.42	3.47	4.32	5.03
Runtime in Seconds	OMP	19.4	21.81	41.52	74.41
	CoSaMP	105.67	119.6	118.11	122.9
	BP	1052.88	1092.5	1044	1083.11
	LASSO	115.7	114	129.96	143.11

sparse coding techniques. Experimental results demonstrate that CoSaMP proves to be a better sparse coding technique in the presence of low noise in most of the cases. OMP has similar results. However at high noise, pre-processing is required as the performance deteriorates for both greedy algorithms and convex techniques. Experimental results indicate that, as the m/k value increases, runtime also increases, particularly for the values of m/k greater than 3. Major drawback of BP is the high computational time, LASSO overcomes this drawback. LASSO proves to be better convex optimization technique than BP. Low computational complexity provides greedy iterative algorithms an edge over convex optimization. From the results, variation in the PSNR with m/k was observed to be small. High PSNR indicates good reconstruction and hence implies a low value of HFEN.

Although performance of greedy algorithms seems to be better than convex solutions in the presence of Rician noise, pre-processing (pre-smoothing) or post processing of the image is required to enhance the quality of the reconstruction. Jittered undersampling can be employed to obtain better denoising in the presence of Rician noise.

References

[1] Saiprasad Ravishankar, and Yoram Bresler, "MR Image Reconstruction from Highly Undersampled k-Space Data by Dictionary Learning", IEEE Transactions on Medical Imaging, Vol. 30, No. 5, pp. 1028-1041, May 2011. https://doi.org/10.1109/TMI.2010.2090538.

[2] M. Lustig, D. L. Donoho, J. M. Santos, and J. M. Pauly, "Compressed sensing MRI", IEEE Signal Processing Mag., Mar. 2008, vol. 25, no. 2, pp. 72–82. https://doi.org/10.1109/MSP.2007.914728.

[3] Saad Qaisar, Rana Muhammad Bilal, Wafa Iqbal, Muqaddas Naureen, and Sungyoung Lee, "Compressive Sensing: From Theory to Applications, a Survey", Journal of Communications and Networks, October 2013, Vol. 15, No. 5. https://doi.org/10.1109/JCN.2013.000083.

[4] J. Tropp, and A. C. Gilbert, "Signal Recovery from Random Measurements via Orthogonal Matching Pursuit", IEEE Transactions on Information Theory, 2007, vol. 53, no.12, pp: 4655-4666. https://doi.org/10.1109/TIT.2007.909108.

[5] D. Needell and J.A. Tropp., "CoSaMP: Iterative signal recovery from incomplete and inaccurate samples". Communications of the ACM, vol. 53, no. 12, December 2010, pp: 93-100. https://doi.org/10.1145/1859204.1859229.

[6] Scott Shaobing Cheny, David L. Donohoz, And Michael A. Saunders, "Atomic Decomposition by Basis Pursuit", Society for Industrial and Applied Mathematics, 1998, Vol. 20, No. 1, pp. 33-61.

[7] Emmanuel Cand`es and Justin Romberg, " -magic: Recovery of Sparse Signals via Convex Programming", Caltech, October 2005.

[8] R. Tibshirani, "Regression shrinkage and selection via the lasso", J. R. Statist. Soc. B, 1996, vol. 58, pp. 267–288. https://doi.org/10.1111/j.2517-6161.1996.tb02080.x.

[9] David Donoho, Victoria Stodden and Yaakov Tsaig, About SparseLab, Stanford University, Version .100, May 2006.

[10] M. Aharon, M. Elad, and A. Bruckstein, "K-SVD: An algorithm for designing overcomplete dictionaries for sparse representation," IEEE Trans. Signal Process., Nov. 2006, vol. 54, no. 11, pp. 4311–4322. https://doi.org/10.1109/TSP.2006.881199.

[11] M.V.R. Manimala, C.D. Naidu and M. N. Giriprasad, "Sparse Recovery Algorithms Based on Dictionary Learning for MR Image Reconstruction", IEEE 2016 International Conference on Wireless Networks, Signal Processing and Networking, March 2016, pp. 1354-1360. https://doi.org/10.1109/WiSPNET.2016.7566358.

[12] Gudbjartsson H, Patz S., "The Rician Distribution on Noisy MRI Data", Magn Reson Med 1995, vol. 34, pp: 910-914. https://doi.org/10.1002/mrm.1910340618.

[13] Gilles Hennenfent and Felix J. Herrmann, "Simply denoise: Wave-field reconstruction via jittered undersampling", Geophysics, May-June 2008, Vol. 73, No. 3, P. V19–V28. https://doi.org/10.1190/1.2841038.
[14] Yang et al., "Brain MR image denoising for Rician noise using pre-smooth non-local means filter", BioMedical Engineering OnLine 2015. https://doi.org/10.1186/1475-925X-14-2.
[15] Javier Portilla, Antonio Tristan-Vega, Ivan W. Selesnick, "Efficient and Robust Image Restoration using Multiple-Feature L2-relaxed Sparse Analysis Priors", IEEE Transactions on Image Processing, December 2015, Vol. 24, No. 12, pp. 5046-5059. https://doi.org/10.1109/TIP.2015.2478405.
[16] Suyash P. Awate and Ross T. Whitaker, "Feature-Preserving MRI Denoising: A Nonparametric Empirical Bayes Approach", IEEE Transactions on Medical Imaging, September 2007, Vol. 26, No. 9, pp. 1242-1255. https://doi.org/10.1109/TMI.2007.900319.
[17] Yue Huangy, John Paisleyy, Qin Lin, Xinghao Dingz, Xueyang Fu and Xiao-ping Zhang, "Bayesian Nonparametric Dictionary Learning for Compressed Sensing MRI", IEEE Transactions on Image Processing, Dec. 2014, Vol. 23, No. 12, pp:5007-5019. https://doi.org/10.1109/TIP.2014.2360122.